Evolving disorder in non-Hermitian lattices

I. Komis, E. T. Kokkinakis, K. G. Makris,* and E. N. Economou
ITCP, Department of Physics, University of Crete, 70013 Heraklion, Greece
and Institute of Electronic Structure and Laser, Foundation for Research and Technology—Hellas (FORTH), P.O. Box 1527, 71110 Heraklion, Greece

(Received 1 December 2025; accepted 30 March 2026; published 29 May 2026)

The impact of disorder on wave transport has been extensively studied in Hermitian systems, where static randomness gives rise to Anderson localization. In non-Hermitian lattices, static disorder can lead to peculiar transport features, including jumpy wave evolution. In contrast, much less is known about how transport is modified when the on-site disorder evolves during propagation. Here, we address this problem by investigating two pertinent non-Hermitian lattice models with disorder altered at regular intervals, characterized by a finite disorder period. In lattices with symmetric couplings and complex on-site disorder, short disorder periods suppress localization and give rise to diffusionlike spreading, while longer periods allow the emergence of jumps. In Hatano-Nelson lattices with real on-site disorder, the non-Hermitian skin effect asymptotically dominates regardless of the disorder strength, while the disorder period reshapes the drift velocity and modulates its competition with Anderson localization. These results establish evolving disorder as a way of tuning non-Hermitian transport.

DOI: 10.1103/4z9l-63lr

I. INTRODUCTION

Disorder constitutes one of the fundamental mechanisms governing wave propagation in complex media. In Hermitian systems, its impact has been studied for more than six decades, with Anderson localization representing the prototypical phenomenon emerging from static randomness [1–5]. Initially formulated in the context of electronic transport, Anderson localization has since been observed in a wide range of platforms, including ultracold atomic gases and acoustic structures [6–9]. Optical systems have also played a central role in this field, providing both theoretical insight and experimental accessibility. Photonic lattices and disordered waveguide arrays, in particular, have established a direct correspondence between disorder-induced localization and optical transport [10–27].

Beyond conservative media, wave dynamics are profoundly modified when the underlying Hamiltonian is non-Hermitian. The introduction of parity-time ($\mathcal{PT}$) symmetry in quantum mechanics [28] established a rigorous framework for extending the notions of eigenvalue reality and phase transitions to non-Hermitian systems. Its implementation in optics, enabled by the interplay of gain and loss, marked the onset of non-Hermitian photonics [29–54]. In parallel, asymmetric coupling between adjacent sites introduced a distinct class of models, first proposed in the Hatano-Nelson system [55], where eigenmodes accumulate at one boundary due to directional transport, an effect now known as the non-Hermitian skin effect [56,57]. The exploration of non-Hermiticity in nonlinear systems [58–70] further illustrates the diversity and ongoing evolution of this area.

Within this broader framework, non-Hermitian photonic lattices provide a natural platform for examining the interplay between disorder and non-Hermiticity. One way to introduce randomness is through complex on-site potentials [71–75], which leads to transport characteristics that differ qualitatively from the Hermitian case, including abrupt transitions known as "Anderson jumps" [76–78]. Interestingly, such jumps were also recently demonstrated in disorder-free non-Hermitian systems [79]. Scaling analyses have clarified the universal aspects of non-Hermitian disorder across models and dimensionalities [80–88]. Other distinctive effects, such as constant-intensity waves that propagate without backscattering [89–93] and scale-free localization exhibiting algebraic or system-size-dependent decay [94–102], further emphasize the richness of transport in non-Hermitian random media.

On the other hand, evolving disorder, where the random parameters change during propagation, introduces fundamentally different transport behavior. In Hermitian media, such time-dependent randomness can profoundly alter interference and localization through mechanisms such as dephasing and Floquet-type driving [103–116]. In contrast, systematic investigations in non-Hermitian systems remain limited, focusing mainly on dephasing processes [117–119], temporally modulated gain-loss profiles [120–122], and stochastically driven light walks [123]. Collectively, these works indicate that deviations from static disorder can strongly modify transport, yet a detailed study of evolving non-Hermitian disorder is still lacking.

*Contact author: makris@physics.uoc.gr

Published by the American Physical Society under the terms of the Creative Commons Attribution 4.0 International license. Further distribution of this work must maintain attribution to the author(s) and the published article's title, journal citation, and DOI.

In this work, we address this problem by examining one-dimensional non-Hermitian lattices subject to evolving random disorder, where the disorder profile is renewed at fixed propagation intervals. Two representative models are considered: lattices with symmetric couplings and evolving complex on-site disorder, and Hatano-Nelson lattices with asymmetric couplings and evolving real disorder. By systematically varying the disorder strength and the disorder period, we show how evolving randomness modifies transport, giving rise to broad spatial spreading, disorder-induced jumps, and boundary accumulation associated with the skin effect. These results establish a general framework for understanding transport in nonconservative systems with evolving disorder.

II. EVOLVING DISORDER IN COMPLEX DISORDERED LATTICES

We begin our analysis by considering a one-dimensional array of N evanescently coupled sites with symmetric nearest-neighbor couplings and on-site potentials $\epsilon_n(z)$ that vary along the propagation coordinate z. Within coupled-mode theory, the field amplitudes $\psi_n(z)$ evolve according to

$$i\,\frac{d\psi_n}{dz} + c\,(\psi_{n+1} + \psi_{n-1}) + \epsilon_n(z)\,\psi_n = 0, \tag{1}$$

where c is the coupling constant and $n = 1, \ldots, N$. Throughout this work, we impose open boundary conditions, $\psi_0 = \psi_{N+1} = 0$. Non-Hermiticity enters through the complex on-site terms $\epsilon_n(z) = \alpha_n(z) + ib_n(z)$, which include both gain and loss.

The disorder evolves as a sequence of piecewise-constant realizations along z. We define update positions $z_a = a\,\ell$, with $a \in \mathbb{N}$ and ℓ denoting the disorder period. Within each interval $z \in [z_a, z_{a+1})$, the on-site potentials are fixed as $\epsilon_n(z) = \epsilon_n^{(a)}$, where each realization $\{\epsilon_n^{(a)}\}$ is drawn independently from a uniform distribution in the complex plane,

$$\alpha_n \in \left[-\tfrac{W_R}{2},\ \tfrac{W_R}{2}\right], \quad b_n \in \left[-\tfrac{W_I}{2},\ \tfrac{W_I}{2}\right]. \tag{2}$$

Here, W_R and W_I represent the real and imaginary disorder strengths. In this work, we set $W_R = W_I \equiv W$ and consider as an initial condition a single-site excitation $\psi_n(0) = \delta_{n,n_0}$, with $n_0 = N/2$ and N even.

To characterize transport, we monitor how the optical power redistributes across the lattice as z increases. Because power is not conserved in non-Hermitian evolution, we define the normalized intensity profile

$$\phi_n(z) = \frac{|\psi_n(z)|^2}{\sum_{k=1}^{N} |\psi_k(z)|^2}. \tag{3}$$

Based on this profile, we define the following statistical moments

$$\langle x^m(z)\rangle = \sum_n n^m\,\phi_n(z). \tag{4}$$

The first moment $\langle x(z)\rangle$ measures the mean position of the wave packet, while the position uncertainty

$$\Delta x(z) = \sqrt{\langle x^2(z)\rangle - \langle x(z)\rangle^2} \tag{5}$$

quantifies its spatial spreading, distinguishing localized from diffusivelike regimes.

During each interval of constant disorder $z \in [z_a, z_{a+1})$, the dynamics are governed by the local Hamiltonian $\hat{H}_a$ corresponding to the on-site potentials $\epsilon_n^{(a)}$. The right and left eigenvalue problems are

$$\hat{H}_a\,|u_{a,j}^R\rangle = \omega_{a,j}\,|u_{a,j}^R\rangle, \quad \hat{H}_a^\dagger\,|u_{a,j}^L\rangle = \omega_{a,j}^*\,|u_{a,j}^L\rangle,$$

with biorthogonality $\langle u_{a,k}^L | u_{a,j}^R\rangle = \delta_{kj}$. The symmetry of $\hat{H}_a$ ($\hat{H}_a = \hat{H}_a^T$) implies $|u_{a,j}^L\rangle^* = |u_{a,j}^R\rangle$. Hence, within this interval the total field can be expanded as

$$|\psi(z)\rangle = \sum_{j=1}^{N} c_{j,0}^{(a)}\, e^{-\mathrm{Im}\,\omega_{a,j}\,(z-z_a)}\, e^{i\,\mathrm{Re}\,\omega_{a,j}\,(z-z_a)}\ |u_{a,j}^R\rangle, \tag{6}$$

where $c_{j,0}^{(a)} = \langle u_{a,j}^L | \psi(z_a)\rangle$ and $|\psi(z_a)\rangle = \sum_{n=1}^{N} \psi_n(z_a)\,|n\rangle$.

Within the interval, each modal projection evolves as $|c_j^{(a)}(z)| = |c_{j,0}^{(a)}|\, e^{-\mathrm{Im}\,\omega_{a,j}\,(z-z_a)}$. A sudden *Anderson jump* [76,77] between distant lattice regions occurs whenever the amplitude of a mode k surpasses that of a previously dominant mode r, satisfying $\mathrm{Im}\,\omega_{a,k} < \mathrm{Im}\,\omega_{a,r}$. In the static limit, $\ell \to \infty$, the on-site potentials remain fixed and the eigenvalue spectrum does not vary with z. In that case, the long-distance evolution is governed by the eigenmode with the smallest imaginary part, $\min_j\{\mathrm{Im}\,\omega_j\}$, corresponding to maximal amplification (or minimal loss).

When the disorder evolves periodically along z, the instantaneous eigenbasis changes at each update. Just before the renewal at z_{a+1}, the field is given by

$$|\psi(z_{a+1}^-)\rangle = \sum_{m=1}^{N} c_{m,0}^{(a)}\, e^{-\mathrm{Im}\,\omega_{a,m}\,\ell}\, e^{i\,\mathrm{Re}\,\omega_{a,m}\,\ell}\ |u_{a,m}^R\rangle. \tag{7}$$

Immediately after the update, the on-site potentials $\epsilon_n^{(a+1)}$ define a new Hamiltonian $\hat{H}_{a+1}$ with eigenbasis $\{|u_{a+1,j}^R\rangle\}$. The field at the beginning of the new interval is then expressed as

$$|\psi(z_{a+1})\rangle = \sum_{j=1}^{N} c_{j,0}^{(a+1)}\ |u_{a+1,j}^R\rangle, \tag{8}$$

where the new projection coefficients follow from

$$\begin{aligned} c_{j,0}^{(a+1)} &= \left\langle u_{a+1,j}^L | \psi(z_{a+1}^-)\right\rangle \\ &= \sum_{m=1}^{N} \mathcal{M}_{a\to a+1}(j,m)\, c_{m,0}^{(a)}\, e^{-\mathrm{Im}\,\omega_{a,m}\,\ell}\, e^{i\,\mathrm{Re}\,\omega_{a,m}\,\ell}, \end{aligned} \tag{9}$$

with $\mathcal{M}_{a\to a+1}(j,m) = \langle u_{a+1,j}^L | u_{a,m}^R\rangle$ denoting the interbasis overlap matrix. This matrix quantifies the projection of the eigenmodes from one disorder segment onto those of the next.

During each subsequent interval $z \in [z_{a+1}, z_{a+2})$, the updated coefficients $c_j^{(a+1)}(z)$ evolve according to the new eigenvalues $\omega_{a+1,j}$. Since both the modal composition (through $\mathcal{M}_{a\to a+1}$) and the gain/loss rates reset at every update, no single mode remains dominant over the entire propagation. Instead, the dynamics consist of a sequence of renewal intervals: Within each, the instantaneous spectrum dictates exponential amplification or dissipation, while at each renewal the field is reprojected onto the eigenbasis of the new Hamiltonian through a nonunitary transformation reflecting the nonorthogonality of the eigenmodes. Consequently, the effective rate of amplification or loss varies along z, governed by the evolving

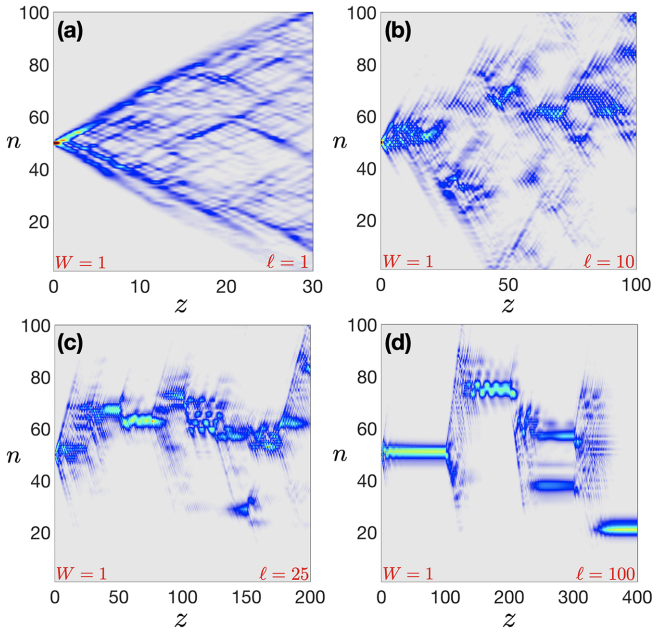


FIG. 1. Weak evolving disorder ($W = 1$): Normalized intensity evolution for four disorder periods: (a) $\ell = 1$, (b) $\ell = 10$, (c) $\ell = 25$, and (d) $\ell = 100$. Each panel corresponds to a single disorder realization. For rapid updates ($\ell = 1$), Anderson localization is suppressed and the wave packet spreads throughout the lattice. As ℓ increases, partial localization develops, and for large disorder periods ($\ell = 100$), distinct Anderson jumps become visible.

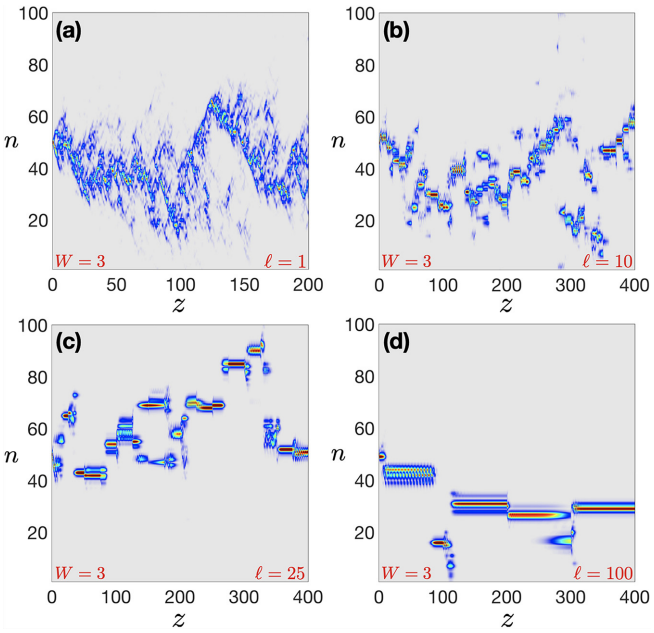


FIG. 2. Intermediate evolving disorder ($W = 3$): Same system as Fig. 1, but for $W = 3$. Each panel corresponds to a single disorder realization. For short disorder periods, the wave packet forms a branching structure of successive jumps across the lattice. Increasing ℓ suppresses these fluctuations and enhances confinement, while at longer periods Anderson jumps dominate the dynamics.

sets $\{\omega_{a,j}\}$ and $\{\mathcal{M}_{a\to a+1}\}$. Unlike the static limit ($\ell \to \infty$), where asymptotic modal selection follows directly from a fixed spectrum, the long-distance behavior in the evolving-disorder case is determined by the entire sequence of update intervals, their duration ℓ, the local eigenvalue distributions, and the overlaps between successive eigenbases.

To elucidate these mechanisms, we first examine representative single disorder realizations before turning to statistical averaging. We consider a lattice of $N = 100$ sites with coupling strength $c = 1$ and analyze individual realizations for three disorder strengths: weak ($W = 1$), intermediate ($W = 3$), and strong ($W = 6$), each studied for four disorder periods $\ell = 1$, 10, 25, 100 as summarized in Figs. 1–3. Before we continue, it is instructive to comment on the Hermitian limit of Eq. (1) (real on-site disorder and symmetric couplings) for comparison. In Hermitian systems, time-evolving disorder is known to suppress Anderson localization when updated sufficiently rapidly, leading to broader spreading compared to the static case. However, Hermitian systems possess purely real spectra and orthogonal eigenmodes, so disorder updates only redistribute modal weights and do not generate jumplike propagation.

For weak disorder ($W = 1$, Fig. 1), frequent updates ($\ell = 1$) suppress Anderson localization, leading to a broad spreading [$\Delta x(z_{\max} = 30) \approx 23$ in Fig. 1(a)]. As the disorder period increases, the potential remains fixed for longer propagation intervals and the wave packet gradually becomes more confined and the propagation crosses over toward localization-dominated dynamics. For $\ell = 100$, the field localizes within a few sites, but each update triggers a sudden reorganization of the dominant eigenmode, producing Anderson jumps and reducing the overall spreading [$\Delta x(z_{\max} = 400) \approx 4$ in Fig. 1(d)].

The intermediate-disorder regime ($W = 3$, Fig. 2) exhibits stronger sensitivity to the disorder period. At $\ell = 1$, the wave packet forms a branching structure, where successive jumps resemble the growth of irregular branches [$\Delta x(z_{\max} = 200) \approx 11$]. As ℓ increases, confinement strengthens and the change of the mean position decreases. For $\ell = 25$ [$\Delta x(z_{\max} = 400) \approx 4$] and $\ell = 100$ [$\Delta x(z_{\max} = 400) \approx 2$], the dynamics are dominated by Anderson jumps, with the packet repeatedly relocating between different lattice regions.

In the strong-disorder regime ($W = 6$, Fig. 3), frequent updates ($\ell = 1$) partially disrupt confinement and again produce a branched pattern [$\Delta x(z_{\max} = 400) \approx 8$]. As the disorder period increases, localization dominates: For $\ell = 25$ and $\ell = 100$, abrupt Anderson jumps persist and the mean uncertainty becomes small [$\Delta x(z_{\max} = 400) \approx 0.57$ in Fig. 3(d)], indicating that localization prevails. While the intensity patterns at intermediate and strong disorder appear qualitatively similar, the corresponding Δx values clearly distinguish the two regimes. In contrast, in the weak-disorder case, localization arises only for large ℓ and remains comparatively weak.

Figures 1–3 thus reveal the dual role of evolving complex disorder. Frequent updates disrupt localization and lead to irregular, diffusionlike spreading, whereas longer disorder periods allow localization to develop, accompanied by Anderson jumps. While single realizations illustrate the underlying mechanisms, they also reveal strong realization-to-realization fluctuations, necessitating statistical averaging to extract

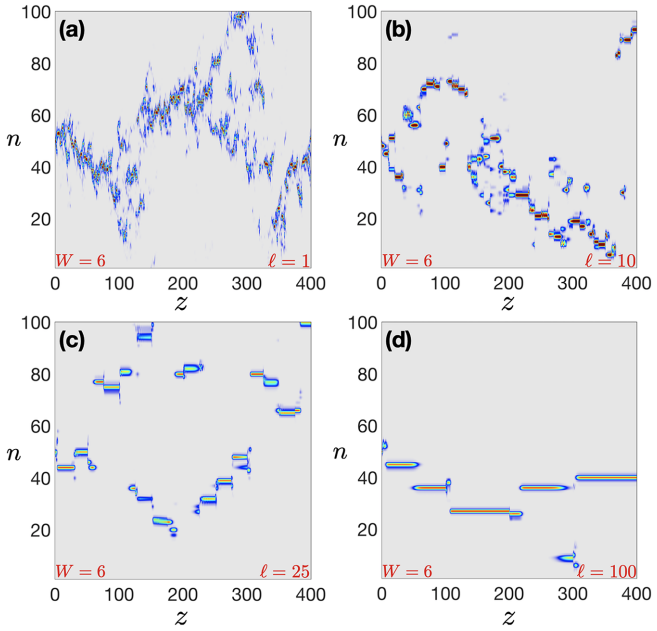


FIG. 3. Strong evolving disorder ($W = 6$): Same system as Fig. 1, but for $W = 6$. Each panel corresponds to a single disorder realization. Although localization dominates, rapid updates ($\ell = 1$) partially disrupt confinement, producing a branching pattern of successive jumps. As ℓ increases, localization strengthens, and for $\ell = 25$ and $\ell = 100$, well-defined Anderson jumps emerge.

robust transport trends. To this end, we compute

$$\overline{\Delta x}(z) = \frac{1}{R}\sum_{r=1}^{R} \Delta x^{(r)}(z), \tag{10}$$

where $\Delta x^{(r)}(z)$ denotes the uncertainty for the r-th realization and R is the ensemble size.

The ensemble-averaged position uncertainty at $z_{\max} = 400$, obtained from $R = 1000$ realizations, is presented in Fig. 4. The diagram confirms and extends the single-realization results: For weak disorder and rapid updates, the averaged uncertainty is large, reflecting diffusive propagation. At intermediate disorder, the transport characteristics depend sensitively on ℓ, reflecting the competition between localization within each interval and disruption at the refresh events. For strong disorder, transport is overall suppressed, although rapid updates still weaken localization. These results identify the disorder period ℓ, which sets the time the random potential remains fixed, as a key control parameter interpolating between broad spatial spreading, jump-dominated dynamics, and Anderson localization. While the article focuses on piecewise-constant disorder updates, we have verified that the transport regimes reported here persist when consecutive disorder realizations are connected smoothly over a finite interpolation window τ.

III. EVOLVING DISORDER IN HATANO-NELSON LATTICES

We now turn to Hatano-Nelson lattices, where non-Hermiticity originates from asymmetric nearest-neighbor couplings that introduce a directional bias in transport. The

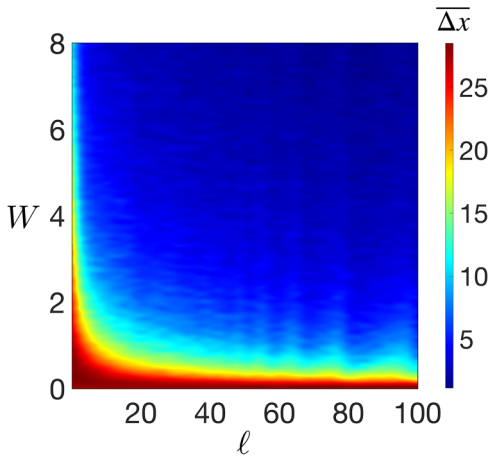


FIG. 4. Long-term uncertainty map: Ensemble-averaged position uncertainty $\overline{\Delta x}(z_{\max})$ as a function of disorder strength W and disorder period ℓ at $z_{\max} = 400$. For weak disorder and rapid updates, transport is diffusionlike with large $\overline{\Delta x}$. At intermediate disorder, $\overline{\Delta x}$ depends strongly on ℓ, reflecting the competition between Anderson localization and evolving disorder. For strong disorder, transport is largely suppressed, although very frequent updates still partially disrupt localization.

field amplitudes evolve according to

$$i\frac{d\psi_n}{dz} + e^{h}\,\psi_{n+1} + e^{-h}\,\psi_{n-1} + \epsilon_n(z)\,\psi_n = 0, \tag{11}$$

with $h > 0$ the asymmetry parameter. In the absence of disorder ($\epsilon_n = 0$), the right eigenmodes under open boundary conditions acquire an exponential envelope and become localized toward the boundary at site $n = 1$, according to our indexing convention, a manifestation of the non-Hermitian skin effect. As before, we consider a single-site excitation $\psi_n(0) = \delta_{n,n_0}$ with $n_0 = N/2$ and N even. In contrast to the complex disordered lattices of the previous section, here the on-site disorder is purely real, $\epsilon_n(z) = \alpha_n(z)$ with $\alpha_n \in [-W/2, W/2]$, drawn independently at each disorder period ℓ and held constant within $[z_a, z_{a+1})$.

Figures 5 and 6 show representative single realizations of propagation dynamics for intermediate ($W = 3$) and strong ($W = 6$) disorder, each examined for four disorder periods, $\ell = 1$, 10, 25, 100. The weak-disorder regime ($W = 1$) is omitted, as the non-Hermitian skin effect dominates across all ℓ and the results are similar for all different realizations.

For intermediate disorder ($W = 3$, Fig. 5), rapid updates ($\ell = 1$) suppress localization and the skin effect governs the dynamics, producing directed transport toward one side of the lattice. As ℓ increases and for the same propagation distance, the mean position remains confined to roughly half of the array, indicating reduced net drift and implying that the wave packet requires longer propagation distances to reach the boundary. For $\ell = 100$ and at the same propagation distance, the dynamics reflect a competition between Anderson localization and the skin effect, although at larger distances the skin effect ultimately dominates.

In the strong-disorder regime ($W = 6$, Fig. 6), this competition is evident at short propagation distances ($\sim$4–5N). For $\ell = 1$, the skin effect dominates and the wave packet drifts toward one edge. At $\ell = 10$, transport remains directed

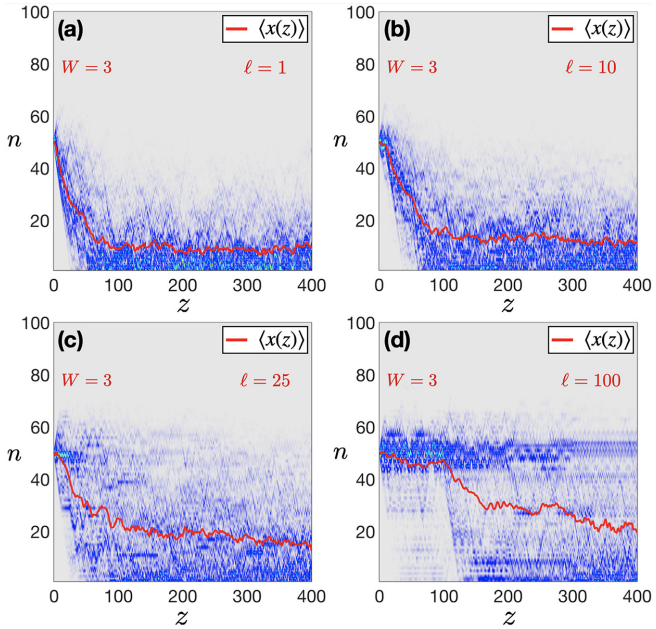


FIG. 5. Hatano-Nelson lattice with intermediate evolving disorder ($W = 3$): Normalized intensity evolution for asymmetry parameter $h = 0.05$ and four disorder periods: (a) $\ell = 1$, (b) $\ell = 10$, (c) $\ell = 25$, and (d) $\ell = 100$. Each panel corresponds to a single disorder realization. The red line indicates the mean position $\langle x(z) \rangle$. For $\ell = 1$, the skin effect dominates and the wave packet is confined near the boundary. As ℓ increases, localization gradually reemerges, broadening the intensity profile over roughly half of the lattice.

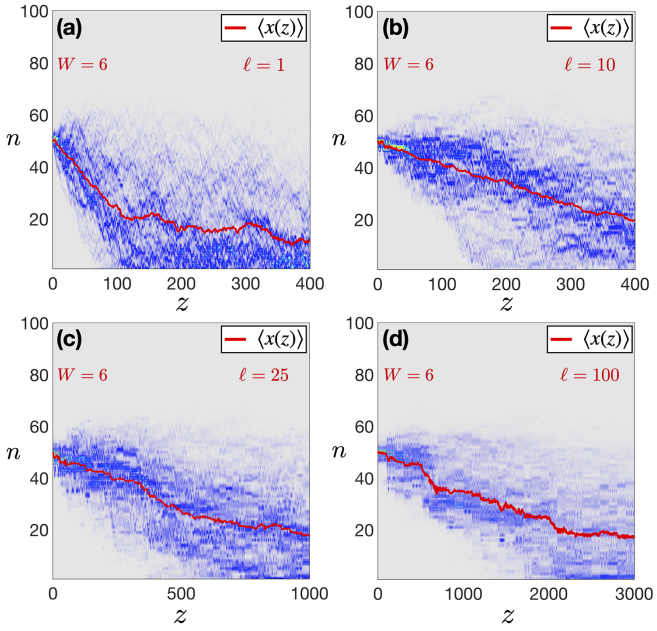


FIG. 6. Hatano-Nelson lattice with strong evolving disorder ($W = 6$): Same system as Fig. 5. Each panel corresponds to a single disorder realization. For $\ell = 1$, rapid updates suppress localization and the skin effect dominates, concentrating intensity at the boundary. As ℓ increases, Anderson localization becomes progressively stronger: Reaching the boundary requires significantly larger propagation distances.

but slows down. For $\ell = 25$ and $\ell = 100$, the skin effect becomes dominant only at large propagation distances, while at short distances ($\sim$4–5N) Anderson localization prevails and confines the intensity near the initial site. Nonetheless, the underlying directionality of transport persists: At sufficiently long propagation distances, the skin effect reemerges. The propagation length required for this transition, and thus the distance needed for the packet to reach the boundary, depends sensitively on both the disorder strength W and the disorder period ℓ, and constitutes a key characteristic of the system dynamics.

It is important to note here that, in contrast to the complex disordered lattices discussed in the previous section, the position uncertainty $\Delta x(z)$ does not capture qualitative differences between disorder periods in the Hatano-Nelson lattice. Due to the persistent boundary-directed drift induced by asymmetric couplings, $\Delta x(z)$ typically exhibits superdiffusive growth for all values of ℓ. For this reason, we characterize transport primarily through the mean displacement and the associated velocity.

The evolving-disorder system lacks a constant drift because the effective bias changes at each update. Thus, to consistently quantify how rapidly the wave approaches the boundary, we adopt a uniform definition across all parameters and realizations: starting from the initially excited site n_0, the velocity is evaluated up to the propagation distance z_{cr} at which the mean position first reaches a fixed fraction $p = 0.2$ of the lattice size,

$$v = \frac{n_0 - \langle x(z_{\mathrm{cr}}) \rangle}{z_{\mathrm{cr}}}, \quad \langle x(z_{\mathrm{cr}}) \rangle = 0.2N, \tag{12}$$

Since the transport in the Hatano-Nelson lattice is directed toward the lower boundary ($n = 1$), this measure captures the characteristic rate at which the excitation advances toward the boundary under evolving disorder. The ensemble velocity $\overline{v}(W, h; \ell)$ is then obtained by averaging over R realizations.

Before applying this velocity measure to the evolving-disorder case, it is instructive to first examine the corresponding behavior under static disorder. As shown in Ref. [75], for a given disorder strength W there exists a finite interval of h values for which an initially localized wave packet remains Anderson localized, either near its initial position or around other lattice regions, and does not fully delocalize toward the preferred boundary, irrespective of the propagation distance. To quantify transport in this regime, we apply the velocity definition of Eq. (12) to the static-disorder case, with the following additional criterion: If the wave packet has not reached $\langle x \rangle = 0.2N$ by $z = 10N$ (a propagation distance sufficiently long to infer asymptotic behavior), we compute the averaged velocity of Eq. (12) using $z_{\mathrm{cr}} = 10N$.

We therefore evaluate the velocity across the entire (W, h) parameter plane, as shown in Fig. 7. For small values of h, increasing the disorder reduces the velocity, consistent with the intuitive expectation that stronger disorder leads to stronger confinement. For larger h, this trend reverses and the velocity counterintuitively increases with W, provided that W is not too large to drive the system into the Anderson-localized regime [124]. Overall, static disorder therefore exhibits two qualitatively distinct transport behaviors, depending on the value of h.

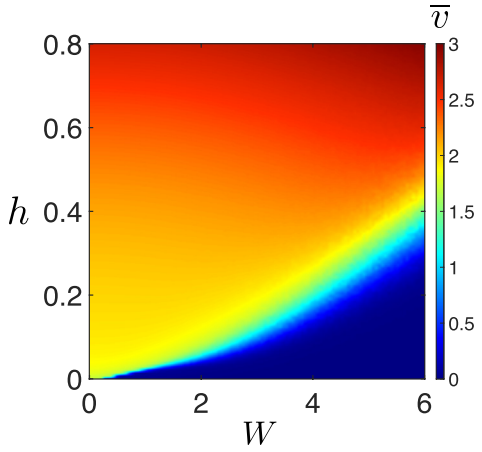


FIG. 7. Velocity map of static disorder: Ensemble-averaged propagation velocity $\overline{v}(W, h)$ in the Hatano-Nelson lattice with static on-site disorder, shown as a function of disorder strength W and asymmetry parameter h. For small h, the velocity decreases with increasing W, as expected, while for larger h the trend reverses and the velocity increases with W, a counterintuitive behavior. This map shows the crossover between these two regimes. Note that we expect very short disorder periods in the evolving case to correspond to an effectively smaller static disorder.

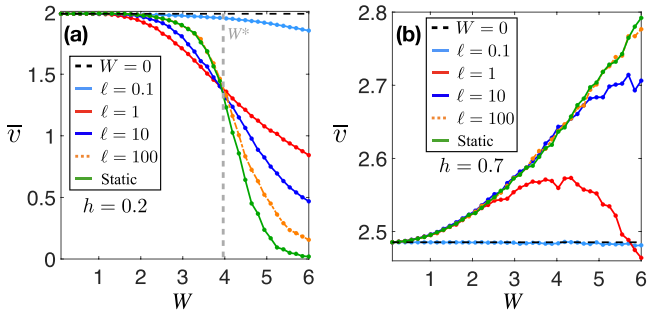


FIG. 8. Propagation velocity vs disorder strength: Ensemble-averaged velocity $\overline{v}(W, h; \ell)$ obtained from the mean position reaching 20% of the lattice, shown for the disorder-free system (black dashed line), the static-disorder case (green line), and four disorder periods $\ell = 0.1$, 1, 10, 100. The very fast-update case $\ell = 0.1$ (light blue) closely follows the disorder-free curve, indicating that rapid updates effectively average out the disorder. (a) For $h = 0.2$, the curves for $\ell = 1$, $\ell = 10$, $\ell = 100$, and static disorder intersect at $W^* \approx 4$. (b) For $h = 0.7$, the static-disorder curve increases with W, as expected from Fig. 7, while the evolving-disorder curves interpolate between the disorder-free and static limits with no common crossing point. Note, however, the nonmonotonic behavior for $\ell = 1$.

Evolving disorder modifies how randomness affects transport in a way that cannot be described by a single disorder strength. For each disorder period ℓ, the system behaves as if it were governed by an effective disorder amplitude $W_{\text{eff}}(\ell)$: Very rapid updates ($\ell \to 0$) average out the random potential and reproduce the disorder-free dynamics, while slow updates approach the static-disorder limit. For intermediate values of ℓ, the correspondence between ℓ and W_{eff} is nontrivial and generally nonmonotonic: decreasing ℓ does not necessarily reduce the influence of disorder, as will be explained in Fig. 9.

Figure 8 shows the ensemble-averaged velocity $\overline{v}(W, h; \ell)$ for $N = 100$, $R = 1000$, $z_{\max} = 1000$, and $p = 0.2$, plotted as a function of disorder strength and two values of asymmetry for several disorder periods. Figure 8(a) is for $h = 0.2$, while Fig. 8(b) is for $h = 0.7$. For $h = 0.2$, the curves for $\ell = 1$, $\ell = 10$, $\ell = 100$, and static disorder intersect at $W^* \approx 4$, a value that also corresponds to the approximate intersection of the velocity curves and is introduced here as an empirical crossover. Below this value, longer disorder periods unexpectedly yield higher velocities, while above it the trend reverses to a more intuitive result: Rapid updates lead to higher velocities. For $h = 0.7$, the static-disorder curve increases with W, in agreement with the results shown in Fig. 7, while the evolving-disorder curves lie between the disorder-free and static limits without sharing a common crossing point.

The role of the period ℓ is clearer when the velocity is plotted directly as a function of ℓ. Figure 9 shows this for $h = 0.2$ and two representative disorder strengths. For $W = 3 < W^*$, the velocity displays a nonmonotonic dependence: for very small ℓ, evolving disorder only weakly perturbs the dynamics and $\overline{v}$ lies slightly above the disorder-free value; as ℓ increases, the influence of disorder becomes stronger and $\overline{v}$ decreases to a minimum near $\ell \simeq 1$–2; For larger ℓ, the dynamics approach the static-disorder limit and $\overline{v}$ increases again. For $W = 5 > W^*$, this behavior disappears: The velocity decreases monotonically with ℓ and approaches the static value as $\ell \to \infty$. These two regimes therefore identify W^* as separating nonmonotonic and monotonic behavior in the dependence of velocity on ℓ.

Taken together, these results show that evolving disorder provides a means of tuning transport in the presence of asymmetric couplings. The disorder period ℓ controls how strongly the instantaneous disorder profile influences the dynamics before it is replaced, leading to either monotonic or nonmonotonic variations of the velocity depending on the relation between (W, h) and the empirical crossing point $W^*(h)$. For all parameter choices where transport is not fully suppressed, the velocity remains finite at sufficiently long propagation

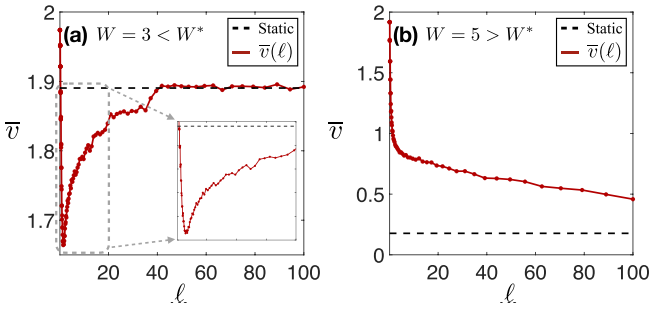


FIG. 9. Propagation velocity vs disorder period: Ensemble-averaged velocity $\overline{v}(\ell)$ for $h = 0.2$ at two representative disorder strengths. (a) For $W = 3 < W^*$, the velocity displays a nonmonotonic dependence on ℓ: It lies slightly above the static-disorder value for very small ℓ, decreases to a minimum near $\ell \simeq 1$–2, and then increases again toward the static-disorder limit. (b) For $W = 5 > W^*$, the velocity decreases monotonically with ℓ and approaches the static value as ℓ increases. These behaviors confirm that W^* marks the threshold separating nonmonotonic and monotonic regimes.

distances, indicating that the directional bias set by the asymmetric couplings prevails asymptotically.

IV. DISCUSSION AND CONCLUSIONS

In conclusion, we have investigated wave dynamics in non-Hermitian lattices with evolving disorder. Two representative systems were analyzed: lattices with symmetric couplings and complex on-site disorder, and Hatano-Nelson lattices with real on-site disorder. The introduction of a finite disorder period ℓ enables a continuous transition between two limiting regimes—static disorder, where Anderson localization dominates, and rapidly evolving disorder, where localization is suppressed and transport becomes spatially broadened.

In lattices with symmetric couplings and complex on-site disorder, single realizations revealed a recurrent sequence of partial localization within each disorder period followed by Anderson jumps at each renewal. Weak disorder favors wave packet spreading, intermediate disorder produces jump-dominated motion, and strong disorder restores Anderson localization unless disrupted by very short periods. In Hatano-Nelson lattices with real on-site disorder, the dynamics reflect a competition between Anderson localization and the non-Hermitian skin effect. The disorder period controls how long localization is allowed to act before the skin directed drift becomes dominant. Short periods suppress localization and enhance boundary-directed drift, while long periods promote localization. The velocity maps reveal crossover points in disorder strength and asymmetry at which the influence of ℓ reverses, separating monotonic from nonmonotonic dependence on the disorder period.

These findings demonstrate that evolving disorder constitutes an efficient mechanism for controlling non-Hermitian transport. By tuning the disorder period ℓ, one can drive the system between broad spatial spreading and Anderson jumps in reciprocal lattices, or modulate the interplay between Anderson localization and the skin effect in Hatano-Nelson lattices. The disorder period therefore emerges as a central control parameter that governs the macroscopic transport behavior. Beyond its fundamental implications, this framework suggests experimentally relevant routes for manipulating wave transport in photonic lattices and opens opportunities for exploring evolving disorder in higher-dimensional and nonlinear settings.

ACKNOWLEDGMENT

The authors acknowledge financial support from the European Research Council (ERC) through the Consolidator Grant Agreement No. 101045135 (Beyond_Anderson).

DATA AVAILABILITY

The data that support the findings of this article are not publicly available. The data are available from the authors upon reasonable request.

[1] P. W. Anderson, Absence of diffusion in certain random lattices, Phys. Rev. **109**, 1492 (1958).
[2] E. Abrahams, P. W. Anderson, D. C. Licciardello, and T. V. Ramakrishnan, Scaling theory of localization: Absence of quantum diffusion in two dimensions, Phys. Rev. Lett. **42**, 673 (1979).
[3] P. A. Lee and T. V. Ramakrishnan, Disordered electronic systems, Rev. Mod. Phys. **57**, 287 (1985).
[4] F. Evers and A. D. Mirlin, Anderson transitions, Rev. Mod. Phys. **80**, 1355 (2008).
[5] C. A. Condat and T. R. Kirkpatrick, Observability of acoustical and optical localization, Phys. Rev. Lett. **58**, 226 (1987).
[6] J. Billy, V. Josse, Z. Zuo, A. Bernard, B. Hambrecht, P. Lugan, D. Clément, L. Sanchez-Palencia, P. Bouyer, and A. Aspect, Direct observation of Anderson localization of matter waves in a controlled disorder, Nature (London) **453**, 891 (2008).
[7] G. Roati, C. D' Errico, L. Fallani, M. Fattori, C. Fort, M. Zaccanti, G. Modugno, M. Modugno, and M. Inguscio, Anderson localization of a non-interacting Bose–Einstein condensate, Nature (London) **453**, 895 (2008).
[8] J. Chabé, G. Lemarié, B. Grémaud, D. Delande, P. Szriftgiser, and J.-C. Garreau, Experimental observation of the Anderson metal–insulator transition with the atomic kicked rotor, Phys. Rev. Lett. **101**, 255702 (2008).
[9] H. Hu, A. Strybulevych, J. H. Page, S. E. Skipetrov, and B. A. van Tiggelen, Localization of ultrasound in a three-dimensional elastic network, Nat. Phys. **4**, 945 (2008).
[10] S. John, Strong localization of photons in certain disordered dielectric superlattices, Phys. Rev. Lett. **58**, 2486 (1987).
[11] K. Busch and C. M. Soukoulis, Transport properties of random media: A new effective medium theory, Phys. Rev. Lett. **75**, 3442 (1995).
[12] D. S. Wiersma, P. Bartolini, A. Lagendijk, and R. Righini, Localization of light in a disordered medium, Nature (London) **390**, 671 (1997).
[13] T. Schwartz, G. Bartal, S. Fishman, and M. Segev, Transport and Anderson localization in disordered two-dimensional photonic lattices, Nature (London) **446**, 52 (2007).
[14] Y. Lahini, A. Avidan, F. Pozzi, M. Sorel, R. Morandotti, D. N. Christodoulides, and Y. Silberberg, Anderson localization and nonlinearity in one-dimensional disordered photonic lattices, Phys. Rev. Lett. **100**, 013906 (2008).
[15] S. Stützer, U. Peschel, C. R. Rosberg, F. Lederer, R. Morandotti, D. N. Christodoulides, and A. Szameit, Anderson cross-localization, Opt. Lett. **37**, 1715 (2012).
[16] S. Karbasi, R. J. Frazier, K. W. Koch, T. Hawkins, J. Ballato, and A. Mafi, Observation of transverse Anderson localization in an optical fiber, Opt. Lett. **37**, 2304 (2012).
[17] G. Pelc, S. Guterman, R. Gutiérrez-Cuevas, A. Goetschy, S. M. Popoff, and Y. Bromberg, Open transmission

channels in multimode fiber cavities with random mode mixing, Phys. Rev. Lett. **135**, 173801 (2025).
[18] D. N. Christodoulides, F. Lederer, and Y. Silberberg, Discretizing light behaviour in linear and nonlinear waveguide lattices, Nature (London) **424**, 817 (2003).
[19] J. Wang and A. Z. Genack, Transport through modes in random media, Nature (London) **471**, 345 (2011).
[20] M. Segev, Y. Silberberg, and D. N. Christodoulides, Anderson localization of light, Nat. Photonics **7**, 197 (2013).
[21] H. H. Sheinfux, Y. Lumer, G. Ankonina, A. Z. Genack, G. Bartal, and M. Segev, Observation of Anderson localization in disordered nanophotonic structures, Science **356**, 953 (2017).
[22] A. Dikopoltsev, S. Weidemann, M. Kremer, A. Steinfurth, H. H. Sheinfux, A. Szameit, and M. Segev, Observation of Anderson localization beyond the spectrum of the disorder, Sci. Adv. **8**, eabn7769 (2022).
[23] Z. Cherpakova, F. Bleckmann, T. Vogler, and S. Linden, Transverse Anderson localization of surface plasmon polaritons, Opt. Lett. **42**, 2165 (2017).
[24] S. Pandey, B. Gupta, S. Mujumdar, and A. Nahata, Direct observation of Anderson localization in plasmonic terahertz devices, Light: Sci. Appl. **6**, e16232 (2017).
[25] J. Duan, S. Xiao, and J. Chen, Anderson localized plasmon in graphene with random tensile-strain distribution, Adv. Sci. **6**, 1801974 (2019).
[26] E. T. Kokkinakis, I. Komis, K. G. Makris, and E. N. Economou, Non-Hermitian off-diagonal disordered optical lattices, Phys. Rev. B **113**, 174210 (2026).
[27] Y. Zhu, H. Jing, R.-W. Peng, C.-Y. Li, J. He, B. Xiong, and M. Wang, Realizing Anderson localization of surface plasmon polaritons and enhancing their interactions with excitons in 2D disordered nanostructures, Appl. Phys. Lett. **116**, 201106 (2020).
[28] C. M. Bender and S. Boettcher, Real spectra in non-Hermitian Hamiltonians having $\mathcal{PT}$ symmetry, Phys. Rev. Lett. **80**, 5243 (1998).
[29] R. El-Ganainy, K. G. Makris, D. N. Christodoulides, and Z. H. Musslimani, Theory of coupled optical $\mathcal{PT}$-symmetric structures, Opt. Lett. **32**, 2632 (2007).
[30] K. G. Makris, R. El-Ganainy, D. N. Christodoulides, and Z. H. Musslimani, Beam dynamics in $\mathcal{PT}$ symmetric optical lattices, Phys. Rev. Lett. **100**, 103904 (2008).
[31] Z. H. Musslimani, K. G. Makris, R. El-Ganainy, and D. N. Christodoulides, Optical solitons in $\mathcal{PT}$ periodic potentials, Phys. Rev. Lett. **100**, 030402 (2008).
[32] A. Guo, G. J. Salamo, D. Duchesne, R. Morandotti, M. Volatier-Ravat, V. Aimez, G. A. Siviloglou, and D. N. Christodoulides, Observation of $\mathcal{PT}$-symmetry breaking in complex optical potentials, Phys. Rev. Lett. **103**, 093902 (2009).
[33] C. E. Rüter, K. G. Makris, R. El-Ganainy, D. N. Christodoulides, M. Segev, and D. Kip, Observation of parity–time symmetry in optics, Nat. Phys. **6**, 192 (2010).
[34] A. Regensburger, C. Bersch, M. A. Miri, G. Onishchukov, D. N. Christodoulides, and U. Peschel, Parity–time synthetic photonic lattices, Nature (London) **488**, 167 (2012).
[35] H. Hodaei, M.-A. Miri, M. Heinrich, D. N. Christodoulides, and M. Khajavikhan, Parity-time–symmetric microring lasers, Science **346**, 975 (2014).
[36] L. Feng, R. El-Ganainy, and L. Ge, Non-Hermitian photonics based on parity–time symmetry, Nat. Photonics **11**, 752 (2017).
[37] R. El-Ganainy, K. G. Makris, M. Khajavikhan, Z. H. Musslimani, S. Rotter, and D. N. Christodoulides, Non-Hermitian physics and $\mathcal{PT}$ symmetry, Nat. Phys. **14**, 11 (2018).
[38] S. K. Özdemir, S. Rotter, F. Nori, and L. Yang, Parity–time symmetry and exceptional points in photonics, Nat. Mater. **18**, 783 (2019).
[39] V. V. Konotop, J. Yang, and D. A. Zezyulin, Nonlinear waves in $\mathcal{PT}$-symmetric systems, Rev. Mod. Phys. **88**, 035002 (2016).
[40] M. A. Miri and A. Alu, Exceptional points in optics and photonics, Science **363**, eaar7709 (2019).
[41] Y. D. Chong, L. Ge, and A. D. Stone, $\mathcal{PT}$-Symmetry breaking and laser-absorber modes in optical scattering systems, Phys. Rev. Lett. **106**, 093902 (2011).
[42] L. Ge, Y. D. Chong, and A. D. Stone, Conservation relations and anisotropic transmission resonances in one-dimensional $\mathcal{PT}$-symmetric photonic heterostructures, Phys. Rev. A **85**, 023802 (2012).
[43] L. Feng, Y.-L. Xu, W. S. Fegadolli, M.-H. Lu, J. E. B. Oliveira, V. R. Almeida, Y.-F. Chen, and A. Scherer, Experimental demonstration of a unidirectional reflectionless parity-time metamaterial at optical frequencies, Nat. Mater. **12**, 108 (2013).
[44] B. Peng, S. K. Ozdemir, F. Lei, F. Monifi, M. Gianfreda, G. L. Long, S. Fan, F. Nori, C. M. Bender, and L. Yang, Parity–time-symmetric whispering-gallery microcavities, Nat. Phys. **10**, 394 (2014).
[45] L. Feng, Z. Jing Wong, R.-M. Ma, Y. Wang, and X. Zhang, Single-mode laser by parity-time symmetry breaking, Science **346**, 972 (2014).
[46] B. Peng, S. K. Özdemir, S. Rotter, H. Yilmaz, M. Liertzer, F. Monifi, C. M. Bender, F. Nori, and L. Yang, Loss-induced suppression and revival of lasing, Science **346**, 328 (2014).
[47] S. Assawaworrarit, X. Yu, and S. Fan, Robust wireless power transfer using a nonlinear parity–time-symmetric circuit, Nature (London) **546**, 387 (2017).
[48] J. Zhang, B. Peng, S. K. Özdemir, K. Pichler, D. O. Krimer, G. Zhao, F. Nori, Y. Liu, S. Rotter, and L. Yang, A phonon laser operating at an exceptional point, Nat. Photonics **12**, 479 (2018).
[49] H. Hodaei, A. U. Hassan, S. Wittek, H. Garcia-Gracia, R. El-Ganainy, D. N. Christodoulides, and M. Khajavikhan, Enhanced sensitivity at higher-order exceptional points, Nature (London) **548**, 187 (2017).
[50] M. P. Hokmabadi, A. Schumer, D. N. Christodoulides, and M. Khajavikhan, Non-Hermitian ring laser gyroscopes with enhanced Sagnac sensitivity, Nature (London) **576**, 70 (2019).
[51] S. Xia, D. Kaltsas, D. Song, I. Komis, J. Xu, A. Szameit, H. Buljan, K. G. Makris, and Z. Chen, Nonlinear tuning of *PT* symmetry and non-Hermitian topological states, Science **372**, 72 (2021).
[52] I. Komis, D. Kaltsas, S. Xia, H. Buljan, Z. Chen, and K. G. Makris, Robustness versus sensitivity in non-Hermitian topological lattices probed by pseudospectra, Phys. Rev. Res. **4**, 043219 (2022).

[53] I. Komis and K. G. Makris, Angular excitation of exceptional points and pseudospectra of photonic lattices, J. Phys. Photonics **6**, 045011 (2024).
[54] E. T. Kokkinakis, I. Komis, K. G. Makris, and E. N. Economou, Non-Hermitian impurity problem, Commun. Phys. **9**, 152 (2026).
[55] N. Hatano and D. R. Nelson, Localization transitions in non-Hermitian quantum mechanics, Phys. Rev. Lett. **77**, 570 (1996).
[56] T. E. Lee, Anomalous edge state in a non-Hermitian lattice, Phys. Rev. Lett. **116**, 133903 (2016).
[57] S. Yao and Z. Wang, Edge states and topological invariants of non-Hermitian systems, Phys. Rev. Lett. **121**, 086803 (2018).
[58] D. A. Dobrykh, A. V. Yulin, A. P. Slobozhanyuk, A. N. Poddubny, and Y. S. Kivshar, Nonlinear control of electromagnetic topological edge states, Phys. Rev. Lett. **121**, 163901 (2018).
[59] C. Hang, D. A. Zezyulin, G. Huang, and V. V. Konotop, Nonlinear topological edge states in a non-Hermitian array of optical waveguides embedded in an atomic gas, Phys. Rev. A **103**, L040202 (2021).
[60] M. Ezawa, Dynamical nonlinear higher-order non-Hermitian skin effects and topological trap-skin phase, Phys. Rev. B **105**, 125421 (2022).
[61] B. Zhu, Q. Wang, D. Leykam, H. Xue, Q. J. Wang, and Y. D. Chong, Anomalous single-mode lasing induced by nonlinearity and the non-Hermitian skin effect, Phys. Rev. Lett. **129**, 013903 (2022).
[62] Y. G. N. Liu *et al.*, Complex skin modes in non-Hermitian coupled laser arrays, Light: Sci. Appl. **11**, 336 (2022).
[63] I. Komis, Z. H. Musslimani, and K. G. Makris, Skin solitons, Opt. Lett. **48**, 6525 (2023).
[64] S. Wang, B. Wang, C. Liu, C. Qin, L. Zhao, W. Liu, S. Longhi, and P. Lu, Nonlinear non-Hermitian skin effect and skin solitons in temporal photonic feedforward lattices, Phys. Rev. Lett. **134**, 243805 (2025).
[65] E. T. Kokkinakis, I. Komis, and K. G. Makris, Self-trapping and skin solitons in two-dimensional non-Hermitian lattices, Commun. Phys. **9**, 22 (2026).
[66] S. Li, M. Hu, J. Lin, C. Fang, Z. Tao, and K. Ding, Soliton transitions mediated by skin-mode localization and band nonreciprocity, arXiv:2508.02311.
[67] B. Many Manda and V. Achilleos, Insensitive edge solitons in a non-Hermitian topological lattice, Phys. Rev. B **110**, L180302 (2024).
[68] S. Longhi, Modulational instability and dynamical growth blockade in the nonlinear Hatano–Nelson model, Adv. Phys. Res. **4**, 2400154 (2025).
[69] H. Ghaemi-Dizicheh, A class of stable nonlinear non-Hermitian skin modes, Phys. Scr. **99**, 125411 (2024).
[70] C. Yuce, Nonlinear skin modes and fixed points, Phys. Rev. B **111**, 054201 (2025).
[71] A. F. Tzortzakakis, K. G. Makris, and E. N. Economou, Non-Hermitian disorder in two-dimensional optical lattices, Phys. Rev. B **101**, 014202 (2020).
[72] Y. Huang and B. I. Shklovskii, Anderson transition in three-dimensional systems with non-Hermitian disorder, Phys. Rev. B **101**, 014204 (2020).
[73] P. O. Sukhachov and A. V. Balatsky, Non-Hermitian impurities in Dirac systems, Phys. Rev. Res. **2**, 013325 (2020).
[74] H. Liu, Z. Su, Z.-Q. Zhang, and H. Jiang, Topological Anderson insulator in two-dimensional non-Hermitian systems, Chin. Phys. B **29**, 050502 (2020).
[75] E. T. Kokkinakis, K. G. Makris, and E. N. Economou, Anderson localization versus hopping asymmetry in a disordered lattice, Phys. Rev. A **110**, 053517 (2024).
[76] A. F. Tzortzakakis, K. G. Makris, A. Szameit, and E. N. Economou, Transport and spectral features in non-Hermitian open systems, Phys. Rev. Res. **3**, 013208 (2021).
[77] A. Leventis, K. G. Makris, and E. N. Economou, Non-Hermitian jumps in disordered lattices, Phys. Rev. B **106**, 064205 (2022).
[78] S. Weidemann, M. Kremer, S. Longhi, and A. Szameit, Coexistence of dynamical delocalization and spectral localization through stochastic dissipation, Nat. Photonics **15**, 576 (2021).
[79] Y. He and T. Ozawa, Anomalous wave-packet dynamics in one-dimensional non-Hermitian lattices, arXiv:2512.07484.
[80] X. Luo, T. Ohtsuki, and R. Shindou, Universality classes of the Anderson transitions driven by non-Hermitian disorder, Phys. Rev. Lett. **126**, 090402 (2021).
[81] K. Kawabata and S. Ryu, Nonunitary scaling theory of non-Hermitian localization, Phys. Rev. Lett. **126**, 166801 (2021).
[82] X. Luo, Z. Xiao, K. Kawabata, T. Ohtsuki, and R. Shindou, Unifying the Anderson transitions in Hermitian and non-Hermitian systems, Phys. Rev. Res. **4**, L022035 (2022).
[83] S. Longhi, Anderson localization in dissipative lattices, Ann. Phys. (Berlin) **535**, 2200658 (2023).
[84] B. P. Nguyen and K. Kim, Transport and localization properties of excitations in one-dimensional lattices with diagonal disordered mosaic modulations, J. Phys. A: Math. Theor. **56**, 475701 (2023).
[85] J.-R. Li, S.-F. Zhang, L.-L. Zhang, and W.-J. Gong, Localization in the one-dimensional quantum chain with nonreciprocal disorder, Phys. Rev. B **110**, 085409 (2024).
[86] I. Komis, K. G. Makris, K. Busch, and R. El-Ganainy, Effect of imaginary gauge on wave transport in driven-dissipative systems, Phys. Rev. A **112**, 043524 (2025).
[87] W.-W. Jin, J. Liu, X. Wang, Y.-R. Zhang, X. Huang, X. Wei, W. Ju, Z. Yang, T. Liu, and F. Nori, Anderson delocalization in strongly coupled disordered non-Hermitian chains, Phys. Rev. Lett. **135**, 076602 (2025).
[88] W. Wang, X. Wang, and G. Ma, Anderson Transition at Complex Energies in One-Dimensional Parity-Time-Symmetric Disordered Systems, Phys. Rev. Lett. **134**, 066301 (2025).
[89] K. G. Makris, A. Brandstotter, P. Ambichl, Z. H. Musslimani, and S. Rotter, Wave propagation through disordered media without backscattering and intensity variations, Light: Sci. Appl. **6**, e17035 (2017).
[90] K. G. Makris, I. Kresic, A. Brandstotter, and S. Rotter, Scattering-free channels of invisibility across non-Hermitian media, Optica **7**, 619 (2020).
[91] I. Komis, S. Sardelis, Z. H. Musslimani, and K. G. Makris, Equal-intensity waves in non-Hermitian media, Phys. Rev. E **102**, 032203 (2020).
[92] C. E. Rivet, A. Brandstötter, K. G. Makris, H. Lissek, S. Rotter, and R. Fleury, Constant-pressure sound waves in non-Hermitian disordered media, Nat. Phys. **14**, 942 (2018).
[93] A. Steinfurth, I. Krešić, S. Weidemann, M. Kremer, K. G. Makris, M. Heinrich, S. Rotter, and A. Szameit, Observation

of photonic constant-intensity waves and induced transparency in tailored non-Hermitian lattices, Sci. Adv. **8**, eabl7412 (2022).
[94] L. Li, C. H. Lee, and J. Gong, Impurity induced scale-free localization, Commun. Phys. **4**, 42 (2021).
[95] C.-X. Guo, X. Wang, H. Hu, and S. Chen, Accumulation of scale-free localized states induced by local non-Hermiticity, Phys. Rev. B **107**, 134121 (2023).
[96] B. Li, H.-R. Wang, F. Song, and Z. Wang, Scale-free localization and $\mathcal{PT}$ symmetry breaking from local non-Hermiticity, Phys. Rev. B **108**, L161409 (2023).
[97] P. Molignini, O. Arandes, and E. J. Bergholtz, Anomalous skin effects in disordered systems with a single non-Hermitian impurity, Phys. Rev. Res. **5**, 033058 (2023).
[98] G.-J. Liu, J.-M. Zhang, S.-Z. Li, and Z. Li, Emergent strength-dependent scale-free mobility edge in a nonreciprocal long-range Aubry-André-Harper model, Phys. Rev. A **110**, 012222 (2024).
[99] W. Li, Z. Sun, Z. Yang, and F. Li, Universal scale-free non-Hermitian skin effect near the Bloch point, Phys. Rev. B **109**, 035119 (2024).
[100] B. Yılmaz, C. Yuce, and C. Bulutay, From scale-free to Anderson localization: A size-dependent transition, Phys. Rev. B **110**, 214206 (2024).
[101] C. Yuce, Scale-free localization: The role of semi-edges, Phys. Scr. **100**, 035009 (2025).
[102] Y. Zhang, L. Su, and S. Chen, Scale-free localization versus Anderson localization in unidirectional quasiperiodic lattices, Phys. Rev. B **111**, L140201 (2025).
[103] D. E. Logan and P. G. Wolynes, Dephasing and Anderson localization in topologically disordered systems, Phys. Rev. B **36**, 4135 (1987).
[104] D. A. Evensky, R. T. Scalettar, and P. G. Wolynes, Localization and dephasing effects in a time-dependent Anderson Hamiltonian, J. Phys. Chem. **94**, 1149 (1990).
[105] J. C. Flores, Diffusion in disordered systems under iterative measurement, Phys. Rev. B **60**, 30 (1999).
[106] H. Yamada and K. S. Ikeda, Dynamical delocalization in one-dimensional disordered systems with oscillatory perturbation, Phys. Rev. E **59**, 5214 (1999).
[107] S. A. Gurvitz, Delocalization in the Anderson model due to a local measurement, Phys. Rev. Lett. **85**, 812 (2000).
[108] J. Košík, V. Bužek, and M. Hillery, Quantum walks with random phase shifts, Phys. Rev. A **74**, 022310 (2006).
[109] A. Schreiber, K. N. Cassemiro, V. Potoček, A. Gábris, I. Jex, and C. Silberhorn, Decoherence and disorder in quantum walks: From ballistic spread to localization, Phys. Rev. Lett. **106**, 180403 (2011).
[110] I. L. Garanovich, S. Longhi, A. A. Sukhorukov, and Y. S. Kivshar, Light propagation and localization in modulated photonic lattices and waveguides, Phys. Rep. **518**, 1 (2012).
[111] J. M. Moix, M. Khasin, and J. Cao, Coherent quantum transport in disordered systems: I. The influence of dephasing on the transport properties and absorption spectra on one-dimensional systems, New J. Phys. **15**, 085010 (2013).
[112] M. Žnidarič and M. Horvat, Transport in a disordered tight-binding chain with dephasing, Eur. Phys. J. B **86**, 67 (2013).
[113] P. L. Krapivsky, J. M. Luck, and K. Mallick, Survival of classical and quantum particles in the presence of traps, J. Stat. Phys. **154**, 1430 (2014).
[114] N. Kamiya, Quantum-to-classical reduction of quantum master equations, Prog. Theor. Exp. Phys. **2015**, 043A02 (2015).
[115] L. Levi, Y. Krivolapov, S. Fishman, and M. Segev, Hyper-transport of light and stochastic acceleration by evolving disorder, Nat. Phys. **8**, 912 (2012).
[116] A. Dikopoltsev, H. Herzig Sheinfux, and M. Segev, Localization by virtual transitions in correlated disorder, Phys. Rev. B **100**, 140202(R) (2019).
[117] S. Longhi, Dephasing-induced mobility edges in quasicrystals, Phys. Rev. Lett. **132**, 236301 (2024).
[118] E. T. Kokkinakis, K. G. Makris, and E. N. Economou, Dephasing-induced jumps in non-Hermitian disordered lattices, Phys. Rev. B **111**, 214204 (2025).
[119] E. T. Kokkinakis, K. G. Makris, and E. N. Economou, Defect-driven incoherent skin localization, Phys. Rev. Res. **8**, L012024 (2026).
[120] S. Wang, C. Qin, W. Liu, B. Wang, F. Zhou, H. Ye, L. Zhao, J. Dong, X. Zhang, S. Longhi, and P. Lu, High-order dynamic localization and tunable temporal cloaking in ac-electric-field driven synthetic lattices, Nat. Commun. **13**, 7653 (2022).
[121] S. Longhi, Delocalization of light in photonic lattices with unbounded potentials, Opt. Lett. **48**, 5293 (2023).
[122] S. Longhi, Algebraic localization–delocalization phase transition in moving potential wells on a lattice, Ann. Phys. (Berlin) **536**, 2300488 (2024).
[123] L. Yu and B. Zhang, Energy variation in stochastically driven light walks [Invited], Opt. Mater. Express **15**, 555 (2025).
[124] Let us note that the velocity definition used in Ref. [75], where the disorder-induced enhancement of velocity in the skin-effect-dominated regime was first reported, differs from the one employed here, leading to minor quantitative discrepancies.